Computers, Materials & Continua
DOI:10.32604/cmc.2021.015421
Article

Tech Science Press

A Highly Efficient Algorithm for Phased-Array mmWave Massive MIMO Beamforming

Ayman Abdulhadi Althuwayb[1], Fazirulhisyam Hashim[2], Jiun Terng Liew[2], Imran Khan[3] Jeong Woo Lee[4], Emmanuel Ampoma Affum[5], Abdeldjalil Ouahabi[6,7,*] and Sébastien Jacques[8]

[1]Department of Electrical Engineering, Jouf University, Sakaka, Aljouf, 72388, Kingdom of Saudi Arabia
[2]Department of Computer and Communication Systems Engineering, Faculty of Engineering, Universiti Putra Malaysia (UPM), Serdang, 43400, Malaysia
[3]Department of Electrical Engineering, University of Engineering and Technology Peshawar, Pakistan
[4]School of Electrical and Electronics Engineering, Chung-Ang University, Seoul, 06974, Korea
[5]Electrical and Electronic Department, Kwame Nkrumah University of Science and Technology, Kumasi, Ghana
[6]UMR 1253, iBrain, Université de Tours, INSERM, Tours, France
[7]LIMPAF Laboratory, Department of Computer Science, University of Bouira, Bouira, 10000, Algeria
[8]University of Tours (France), GREMAN UMR 7347, CNRS, INSA Centre Val-de-Loire, Tours, 37100, France
[*]Corresponding Author: Abdeldjalil Ouahabi. Email: ouahabi@univ-tours.fr
Received: 20 November 2020; Accepted: 30 December 2020

Abstract: With the rapid development of the mobile internet and the internet of things (IoT), the fifth generation (5G) mobile communication system is seeing explosive growth in data traffic. In addition, low-frequency spectrum resources are becoming increasingly scarce and there is now an urgent need to switch to higher frequency bands. Millimeter wave (mmWave) technology has several outstanding features—it is one of the most well-known 5G technologies and has the capacity to fulfil many of the requirements of future wireless networks. Importantly, it has an abundant resource spectrum, which can significantly increase the communication rate of a mobile communication system. As such, it is now considered a key technology for future mobile communications. MmWave communication technology also has a more open network architecture; it can deliver varied services and be applied in many scenarios. By contrast, traditional, all-digital precoding systems have the drawbacks of high computational complexity and higher power consumption. This paper examines the implementation of a new hybrid precoding system that significantly reduces both calculational complexity and energy consumption. The primary idea is to generate several sub-channels with equal gain by dividing the channel by the geometric mean decomposition (GMD). In this process, the objective function of the spectral efficiency is derived, then the basic tracking principle and least square (LS) techniques are deployed to design the proposed hybrid precoding. Simulation results show that the proposed algorithm significantly improves system performance and reduces computational complexity by more than 45% compared to traditional algorithms.

Keywords: 5G; mmWave; phased array; algorithm; antenna beamforming

1 Introduction

As the number of wireless devices continues to grow and wireless applications continue to expand, user demand for wireless network transmission rates continues to increase. The existing low frequency network (<3 GHz) is struggling to meet this increasing demand for speed. Addition, it is oriented towards greater bandwidth. High frequency resources are currently being studied and implemented [1] and the 60 GHz millimeter wave (mmWave) has aroused the interest of a large number of researchers. Many countries have opened unlicensed 60 GHz mmWave frequency bands for research and testing. For example, China's open frequency band is 59∼64 GHz, in the United States the band is 57∼64 GHz, and Japan uses 59∼66 GHz. Relevant standards have been established to promote the industrialization of 60 GHz mmWave applications [2–6]. Wireless HD (WiHD) is primarily used to achieve high-quality, high-definition, uncompressed video transmission indoors, while the IEEE802.15.3c standard is primarily used for high-quality indoor networks. Wireless personal area network (WPAN) applications and the IEEE802.11.ad standard provide high-quality wireless local area network (WLAN) applications [7].

The application of the 60 GHz mmWave band presents significant challenges. Oxygen attenuation on the ground reaches 15 dB/km as a result of the oxygen attenuation window. In addition, reflection attenuation and other losses occur as part of the propagation process. As such, the link budget is very limited and if we are in a non-line-of-sight (NLOS) environment, the performance of the link will be severely affected [8]. Furthermore, the output power of the power amplifier in the 60 GHz mmWave frequency band is very limited. Therefore, exploitation of the short wavelength region and small antenna arrays in this frequency band, as well as the use of beamforming technology, can help improve link gain. In terms of implementation methods, beamforming technology can be divided into adaptive beamforming and fixed beamforming [9]. Although adaptive beamforming technology performs well, the complexity of its implementation is high. The implementation of codebook-based fixed beamforming technology is not very complex, but unfortunately it is not very efficient. In terms of hardware architecture, digital beamforming technology is generally used. Each antenna is configured with a radio frequency link, which sees high costs and power consumption [10]. MmWave generally adopts radio frequency beamforming technology and realizes the alignment of the transceiver through the radio frequency phase shifter to directly adjust the signal, reducing the cost [11,12]. MmWave beamforming technology has been the subject of numerous studies. The IEEE802.11.ad and IEEE802.15.3c standards both adopt codebook-based beamforming technology as part of the RF phase-shifting architecture and find an optimal beam through hierarchical searching [13–16].

In recent years, mmWave massive multiple-input multiple-output (massive-MIMO) technology has attracted the attention of the scientific community. This is primarily because mmWave communications present an abundant spectrum and hybrid massive-MIMO precoding technology provides a higher beam gain and compensates for the propagation defect of the high loss of mmWave communications [17]. However, at the same time, the scale of the hardware required and the complexity of encoding and decoding are both increasing and a new hybrid precoding scheme is needed to reduce system complexity.

MIMO multiplexing systems typically use singular value decomposition (SVD) to obtain several independent orthogonal spatial sub-channels for higher throughput. However, due to the large differences in the gain of each sub-channel in this method, it is necessary to use different codecs and modulation/demodulation methods to meet the bit error rate (BER) requirements, making the system very complex [18]. For this reason, the authors of [19] propose a scheme based on geometric mean decomposition (GMD). This scheme decomposes the Rayleigh fading channel

under orthogonal frequency division multiplexing into several parallel sub-channels with equal channel gains. This helps to avoid complicated bit allocation and power loading processes and reduces the difficulty of system encoding and decoding, reducing overall system complexity [20]. In order to obtain a hybrid precoding scheme with the best frequency efficiency, the authors in [21] transformed the frequency efficiency optimization problem into a sparse approximation problem and optimized it using the orthogonal matching pursuit (OMP) algorithm to downlink the frequency efficiency of a single-user MIMO system [22]. The authors of [23] studied the frequency efficiency of a single-user MIMO system and designed a hybrid precoding scheme, proposing an algorithm to optimize the frequency efficiency of the system. However, they only considered the optimization of the algorithm and did not proceed in terms of the complexity of the coding and decoding of the system. After studying MIMO channel diagonalization, the authors of [24] used the GMD method to efficiently compensate for gain difference defects in SVD-weighted sub-channels. The authors of [25] examined the impact of the differential GMD precoder on the frequency efficiency of the system based on the assumption of a low feedback rate in single-user MIMOs, but the relationship between the frequency efficiency of the system and the number of BS antennas and the signal-to-noise ratio remains unclear and would be difficult to promote in the current communications environment.

Based on the current state of research on the spectral efficiency of the millimeter wave MIMO downlink system, the GMD channel processing method was applied to the processing of Saleh-Valenzuela mmWave channels. Compared to the traditional SVD algorithm, the complexity of the system can be effectively reduced and, for the single-user mobile downlink communication scenario, the hybrid GMD-based precoding scheme is proposed and implemented. This scheme can give good results, assuming that the system complexity can be reduced and the spectral efficiency can be improved.

2 System Modeling

2.1 Hybrid Precoding Model

Fig. 1 shows the proposed modeling of the mmWave Massive-MIMO system. To simplify the analysis, the system only takes into account the downlink transmission scenario of a single cell and a single user. The base station is configured with N_t antennas and N_t^{RF} radio frequency chains; the transmission data contains N_s data streams and satisfies the following in equation: $N_s \le N_t^{RF} \le N_t$. The user receiver is configured with N_r antennas and N_r^{RF} radio frequency chains to meet the following requirement: $N_s \le N_r^{RF} \le N_r$.

The hybrid precoding, which is performed at the base station, consists of digital precoding, $P_D \in \mathbb{C}^{N_t^{RF} \times N_s}$, and analog precoding, $P_A \in \mathbb{C}^{N_t \times N_t^{RF}}$. The precoding of the corresponding base station is defined as follows: $P = P_A P_D$. Assuming that the base station sends a signal vector of s, then the hybrid precoding signal is expressed by (1).

$$x = Ps = P_A P_D s \tag{1}$$

where P is the base station transmit power, which satisfies $\mathrm{tr}\left\{PP^H\right\} \le N_s$. Consequently, the signal vector received by the user is expressed by (2).

$$y = \sqrt{\rho} H P_A P_D s + n \tag{2}$$

In the previous equations, $(\cdot)^H$ is the complex conjugate transposition operation; ρ is the mean received power; $H \in \mathbb{C}^{N_r \times N_t}$ is the transmission matrix of the mmWave channel; $n \in \mathbb{C}^{N_r \times 1}$

is the noise vector, which obeys the complex Gaussian distribution, i.e., $CN\left(0,\sigma^2 I_{N_\mathrm{r}}\right)$, where σ^2 is the noise variance, I_{N_r} is the unit dimensional matrix $N_\mathrm{r} \times N_\mathrm{r}$. The analog precoding P_A is implemented by a network of phase shifter, and respects the limit of the constant modulus, i.e., $\left|\{P_\mathrm{A}\}_{i,j}\right| = 1/N_\mathrm{t}$, where $\{\cdot\}_{i,j}$ is the element on the i-th row and j-th column of the matrix; $|\cdot|$ is the modulus of the complex numbers.

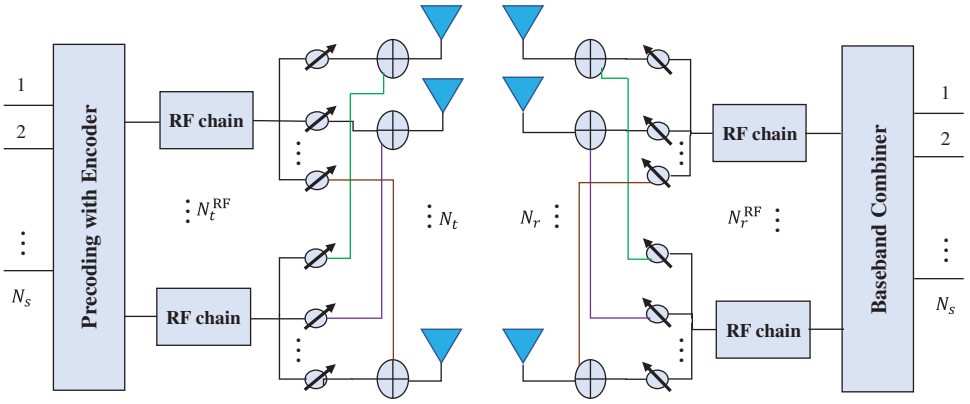

Figure 1: Proposed system model

2.2 Channel Model

The mmWave channel follows the Saleh Valenzuela channel model, and the channel transfer matrix H can be expressed by (3) [26].

$$H = \sqrt{\frac{N_\mathrm{t} N_\mathrm{r}}{L}} \sum_{i}^{L} \beta_i \alpha_r\left(\Phi_i^r\right) \alpha_t\left(\Phi_i^t\right) \tag{3}$$

In (3), L is the number of (resolvable) channel paths, β_i is the complex gain of the i-th path, and Φ_i^r and Φ_i^t are respectively the arrival angle (AoA) and departure angle (AoD) of the i-th path. $\alpha_r\left(\Phi_i^r\right)$ and $\alpha_t\left(\Phi_i^t\right)$ are response vectors of the antenna array of the user's receiver corresponding to Φ_i^r and the base station transmitter corresponding to Φ_i^t.

For a simple uniform linear array (ULA) containing N elements, the array response vector is expressed as:

$$\vartheta^{\mathrm{ULA}}(\Phi) = \sqrt{\frac{1}{N}}\left[1, e^{jkd\sin(\Phi)}, e^{j2kd\sin(\Phi)}, \ldots, e^{j(N-1)kd\sin(\Phi)}\right]^{\mathrm{T}} \tag{4}$$

In (4), $k = 2\pi/\lambda$, λ is the wavelength and d is the separation distance of the antenna. Due to the limited spatial scattering in mmWave propagation, the corresponding mmWave massive MIMO channel matrix is a lower rank matrix, so that a near-optimal system spectral efficiency can be achieved with a limited radio frequency (RF) chain [27].

3 Proposed Algorithm

3.1 Problem Description

The limited spatial scattering of the propagating mmWave considerably varies the singular value of the channel matrix H [28]. As shown in Fig. 2a, this results in a large difference in the signal-to-noise ratio (SNR) of the different sub-channels after power allocation.

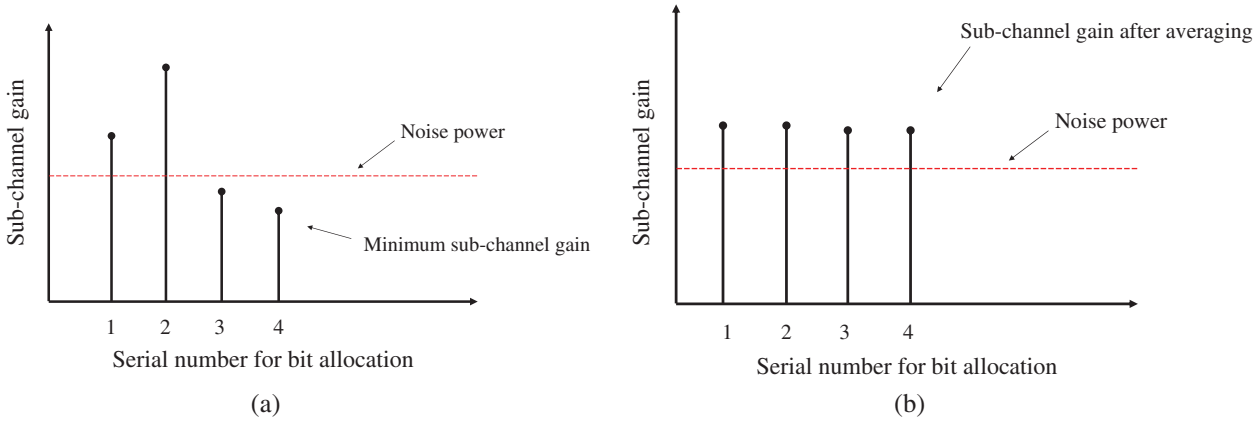

Figure 2: Illustration of sub-channel gain. (a) traditional SVD precoding; (b) GMD precoding

In the same modulation/demodulation mode, the bit error rate (BER) of all sub-channels is determined by the sub-channel with the lowest fixed SNR. In order to ensure that all sub-channels maintain a similar bit error rate, the SVD-based precoding system requires careful bit allocation for each sub-channel, which will greatly increase the complexity of the system encoding/decoding process [29]. However, the H-channel adopts the GMD technique to effectively equalize the SNR of each sub-channel [24,25]. As shown in Fig. 2b, this avoids the complicated process of allocating bits and loading power into the sub-channels, and reduces the complexity of programming and decoding the system. The overall complexity of the system is thus reduced. On this basis, the design relies on the GMD hybrid precoding optimization matrix, to achieve the optimized value of spectral efficiency under the lower complexity of coding, decoding and modulation, and demodulation.

From (2), the spectral efficiency of the system is defined by (5) [30].

$$R = \log\left[\det\left(I + \frac{\rho}{N_s\sigma_n^2} H P_A P_D P_D^H P_A^H H^H\right)\right] \tag{5}$$

3.2 Optimization of Spectral Efficiency

From (5), we can see that for any arbitrary value having a rank of N_s and a singular value of $\sigma_1 \geq \sigma_2 \geq \ldots \geq \sigma_{N_s}$. The complex channel matrix H can be expressed by (6).

$$H = G^{GMD} R^{GMD} Q_{GMD}^H = [G_1 G_2] \begin{bmatrix} R_1 & * \\ 0 & R_2 \end{bmatrix} \begin{bmatrix} Q_1^H \\ Q_2^H \end{bmatrix} \tag{6}$$

In (6), $G^{\mathrm{GMD}}=[G_1 G_2]\in\mathbb{C}^{N_r\times N_t}$, $G_1\in\mathbb{C}^{N_r\times N_s}$ is a positive semi-definite matrix containing the unitary matrix G^{GMD} containing the N_s column vector from the left; $Q_{\mathrm{GMD}}^{\mathrm{H}}=\begin{bmatrix}Q_1^{\mathrm{H}}\\ Q_2^{\mathrm{H}}\end{bmatrix}$ is a unitary matrix, $Q_1\in\mathbb{C}^{N_t\times N_s}$ is a positive semi-definite matrix containing the N_s column vector from the left of the unitary matrix Q_{GMD}; $R^{\mathrm{GMD}}=\begin{bmatrix}R_1 & *\\ 0 & R_2\end{bmatrix}\in\mathbb{C}^{N_r\times N_t}$ is a diagonal matrix with singular values of matrix H. $R_1\in\mathbb{C}^{N_s\times N_s}$ is an upper triangular matrix with the same diagonal elements, and its diagonal elements contain the geometric mean of the first N_s singular values of matrix H. That is, $\forall i$, where $r_{i,i}=\left(\sigma_1,\sigma_2,\ldots,\sigma_{N_s}\right)^{\frac{1}{N_s}}=\overline{r}$ holds, $r_{i,i}$ is equivalent to the parallel subchannel gain after GMD processing, $\sigma_1,\sigma_2,\ldots,\sigma_{N_s}$ is the singular value of H. $R_2\in\mathbb{C}^{(N_r-N_s)\times(N_t-N_s)}$ is a triangular matrix, and its diagonal elements are the singular values of matrix H after N_s, and the corresponding matrix elements are arbitrary values. The * denotes any random possible value within the matrix set. As there are only N_s transmission data streams, only the geometric mean of the first N_s singular values is taken into account here.

From (6), the H-channel matrix will be processed by GMD, and the processed efficiency can be expressed by (7).

$$R=\log\left[\det\left(I+\frac{\rho}{N_s\sigma_n^2}\left(R^{GMD}\right)^2 Q_{GMD}^H P_A P_D P_D^H P_A^H Q_{GMD}\right)\right] \tag{7}$$

Assuming that $P=P_A P_D$ is very close to the optimal unit matrix $Q_{\mathrm{res}}=Q_1$, the following two approximate conclusions can be obtained [6]:

(1) The matrix $I_{N_s}-Q_1^{\mathrm{H}}P_A P_D P_D^{\mathrm{H}}P_A^{\mathrm{H}}Q_1$ has a small eigenvalue. It can thus be expressed in a way equivalent to $Q_1^{\mathrm{H}}P_A P_D\approx I_{N_s}$ in precoding mmWave.

(2) Moreover, since the singular value of $Q_2^{\mathrm{H}}P_A P_D$ is low, it can be equivalent to $Q_1^{\mathrm{H}}P_A P_D\approx 0$, resulting in the transformation formula defined by (8).

$$Q_{GMD}^H P_A P_D P_D^H P_A^H Q_{GMD}=\begin{bmatrix}Q_1^H P_A P_D P_D^H P_A^H Q_1 & Q_1^H P_A P_D P_D^H P_A^H Q_2\\ Q_2^H P_A P_D P_D^H P_A^H Q_1 & Q_2^H P_A P_D P_D^H P_A^H Q_2\end{bmatrix}=\begin{bmatrix}Q_{11} & Q_{12}\\ Q_{21} & Q_{22}\end{bmatrix} \tag{8}$$

Substituting Eq. (8) into Eq. (7), we obtain Eq. (9).

$$\begin{aligned}R&=\log\left[\det\left(I+\frac{\rho}{N_s\sigma_n^2}\begin{bmatrix}R_1^2 & *\\ 0 & R_2^2\end{bmatrix}\begin{bmatrix}Q_{11} & Q_{12}\\ Q_{21} & Q_{22}\end{bmatrix}\right)\right]\approx\log\left[\det\left(I_{N_s}+\frac{\rho}{N_s\sigma_n^2}R_1^2 Q_1^{\mathrm{H}}P_A P_D P_D^{\mathrm{H}}P_A^{\mathrm{H}}Q_1\right)\right]\\ &=\log\left[\left|I_{N_s}+\frac{\rho}{N_s\sigma_n^2}R_1^2\right|\right]-\left(N_s-\left\|Q_1^{\mathrm{H}}P_A P_D\right\|_{\mathrm{F}}^2\right)\end{aligned} \tag{9}$$

In (9), the first term can be obtained by setting $Q_{\mathrm{res}}=R_1$, and the second term is the squared chord distance between two points $Q_{\mathrm{res}}=R_1$ and $(P_A P_D)$ on the distance of the Grassmann manifold coconut $\|Q_{\mathrm{res}}-Q_A Q_D\|_{\mathrm{F}}$. Therefore, the problem of maximizing the spectral efficiency can be converted into that of minimizing $\|Q_{\mathrm{res}}-Q_A Q_D\|_{\mathrm{F}}$.

Assuming that Q_{res} is the optimal precoding based on GMD, and that Q_A and Q_D are respectively the corresponding analog precoding and digital precoding, the optimized objective function after transformation is defined by (10).

$$\left(Q_A^{\text{opt}}, G_D^{\text{opt}}\right) = \underset{Q_A, Q_D}{\arg\min} \| Q_{\text{res}} - Q_A Q_D \|_{\text{F}}$$

$$\text{s.t.} \quad \left|\{Q_A\}_{i,j}\right| = \frac{1}{\sqrt{N_{\text{t}}}},$$

$$\text{tr}\left(Q_A Q_D Q_D^{\text{H}} Q_A^{\text{H}}\right) \le N_{\text{s}} \tag{10}$$

3.3 *Conversion Optimization Objective Function*

To reduce the complexity of the GMD transformation and obtain the optimized solution of Eq. (10), the optimization problem can be transformed by Lemma 1.

Lemma 1: Suppose the SVD of the channel matrix H is defined by (11).

The singular values of the channel matrix are arranged in descending order, then there is a unit matrix $S_{\text{R}} \in \mathbb{C}^{N_{\text{s}} \times N_{\text{s}}}$, $S_{\text{L}} \in \mathbb{C}^{N_{\text{s}} \times N_{\text{s}}}$ such that $Q_1 = V_1 S_{\text{R}}$; $G_1 = U_1 S_{\text{L}}$; $R_1 = S_{\text{L}}^{\text{T}} \sum_1 S_{\text{R}}$.

$$H = U \sum V^{\text{H}} = [U_1 U_2] \begin{bmatrix} \sum_1 & 0 \\ 0 & \sum_2 \end{bmatrix} \begin{bmatrix} V_1^{\text{H}} \\ V_2^{\text{H}} \end{bmatrix} \tag{11}$$

Lines of evidence: Calculate the geometric mean of the channel matrix $\overline{r} = \left(\sigma_1, \sigma_2, \ldots, \sigma_{N_{\text{s}}}\right)^{\frac{1}{N_{\text{s}}}}$, define the auxiliary matrix by (12).

$$R_1 := \left\{M^{(i)}\right\}^{\text{H}} R_1 M^{(i)}, \quad Q_1 := Q_1 M^{(i)}, \quad G_1 := G_1 M^{(i)} \tag{12}$$

In the previous equation, ":=" means is defined as, and $M^{(i)}$ is the corresponding permutation matrix. Let $R_1 = \sum_1$, $Q_1 = V_1$, $G_1 = U_1$, and define 2 replacements from $I_{N_{\text{s}}}$ containing 4 elements $\left\{N_{\text{L}}^{(i)}\right\}_{i,i}$, $\left\{N_{\text{L}}^{(i)}\right\}_{i+1,i}$ $\left\{N_{\text{L}}^{(i)}\right\}_{i,i+1}$, $\left\{N_{\text{L}}^{(i)}\right\}_{i+1,i+1}$ sub-matrix generation. The four elements of the matrices $N_{\text{L}}^{(i)}$, $N_{\text{R}}^{(i)}$ have the following two-dimensional matrix form (see (13)).

$$\ddot{\theta}_L^{(i)} = \frac{1}{\overline{r}} \begin{bmatrix} cr_{i,i} & sr_{i+1,i+1} \\ -sr_{i+1,i+1} & cr_{i,i} \end{bmatrix},$$

$$\ddot{\theta}_R^{(i)} = \begin{bmatrix} c & -s \\ s & c \end{bmatrix} \tag{13}$$

where $r_{i,i} = r_{i+1,i+1} = \overline{r}$, when $c = 1$, $s = 0$, then $r_{i,i} \ne r_{i+1,i+1}$, therefore:

$$c = \sqrt{\frac{\overline{r}^2 - r_{i+1,i+1}^2}{r_{i,i}^2 - r_{i+1,i+1}^2}}, \quad s = \sqrt{1 - c^2} \tag{14}$$

Update R_1, Q_1 and G_1, then:

$$R_1 := N_L^{(i)} R_1 N_R^{(i)}, \quad Q_1 := Q_1 \left\{ N_L^{(i)} \right\}^T, \quad G_1 := G_1 N_R^{(i)} \tag{15}$$

Further:

$$R_1^{i+1} = \ddot{\theta}_L^{(i)} \begin{bmatrix} r_{i,i} & 0 \\ 0 & r_{i+1,i+1} \end{bmatrix} \ddot{\theta}_R^{(i)} = \begin{bmatrix} \overline{r} & * \\ 0 & \frac{r_{i,i} r_{i+1,i+1}}{\overline{r}} \end{bmatrix} \tag{16}$$

This shows that through $N_{\mathrm{L}}^{(i)} R_1 N_{\mathrm{R}}^{(i)}$, we can make $r_{i,i} = \overline{r}$, and keep the other elements unchanged. Substitute R_i for R_1 in the calculation in turn, where $1 \le i \le N_{\mathrm{s}} - 1$.

Eq. (15) shows that $M^{(i)}$, $N_{\mathrm{L}}^{(i)}$ and $N_{\mathrm{R}}^{(i)}$ are all unitary matrices, and Eq. (16) shows that only the value of diagonal elements is changed through GMD transformation, and other elements remain unchanged. Therefore, the matrix $S_{\mathrm{L}} = M^{(1)} N_{\mathrm{R}}^{(1)} M^{(2)} N_{\mathrm{R}}^{(2)} \ldots M^{(N_{\mathrm{s}})} N_{\mathrm{R}}^{(N_{\mathrm{s}})}$ and $S_{\mathrm{R}} = M^{(1)} \left(N_{\mathrm{L}}^{(1)} \right)^{\mathrm{T}} M^{(2)} \left(N_{\mathrm{L}}^{(2)} \right)^{\mathrm{T}} \ldots M^{(N_{\mathrm{s}})} \left(N_{\mathrm{L}}^{(N_{\mathrm{s}})} \right)^{\mathrm{T}}$, substituting into Eq. (15), we get $R_1 = S_{\mathrm{L}}^{\mathrm{T}} \sum_1 S_{\mathrm{R}}$. Similarly, $Q_1 = V_1 S_{\mathrm{R}}$; $G_1 = U_1 S_{\mathrm{L}}$. Hence, Lemma 1 is proved.

According to Lemma 1, the right side of Eq. (10) can be rewritten as (17).

$$\| Q_{\mathrm{res}} - Q_A Q_D \|_{\mathrm{F}} = \| R_1 - Q_A Q_D \|_{\mathrm{F}} = \| V_1 S_{\mathrm{R}} - Q_A Q_D \|_{\mathrm{F}} = \left\| V_1 - Q_A Q_D \{ S_{\mathrm{R}} \}^{\mathrm{H}} \right\|_{\mathrm{F}} \tag{17}$$

The condition that the third step of the Eq. (17) holds is because the F-norm remains unchanged under the matrix rotation, and there is a $\widetilde{Q}_D = Q_D \{ S_{\mathrm{R}} \}^{\mathrm{H}}$.

Substituting Eq. (17) into Eq. (10), we can get (18).

$$\begin{aligned} &\left(Q_A^{\mathrm{opt}}, G_D^{\mathrm{opt}} \right) = \underset{Q_A, \widetilde{Q}_D}{\arg\min} \left\| V_1 - Q_A \widetilde{Q}_D \right\|_{\mathrm{F}} \\ &\text{s.t.} \left| \{ Q_A \}_{i,j} \right| = \frac{1}{\sqrt{N_{\mathrm{t}}}}, \\ &\mathrm{tr} \left(Q_A \widetilde{Q}_D Q_D^{\mathrm{H}} \widetilde{Q}_A^{\mathrm{H}} \right) \le N_{\mathrm{s}} \end{aligned} \tag{18}$$

So far, the objective function (i.e., Eq. (10)) has been effectively transformed.

3.4 Optimize Objective Function Solution

From (18), although Q_A and Q_D are coupled to each other, because the elements of Q_A have constant modulus constraints, Q_A and Q_D can be designed separately by decoupling, i.e., when designing Q_A, Q_D remains unchanged [21]. The reverse is also true because the constant modulus elements of $\alpha_t \left(\Phi_i^t \right)$ satisfy the constraint of $\left| \{ Q_A \}_{i,j} \right| = \frac{1}{\sqrt{N_{\mathrm{t}}}}$, and the column vector of V_1 forms the orthogonal base of the channel row vector space, so that V_1 can be considered as a linear combination of $\alpha_t \left(\Phi_i^t \right)$. By approximating V_1 by Q_A and Q_D, the optimal solution of Q_A and Q_D can be obtained. For this reason, it is necessary to reasonably find the "optimal" N_t^{RF} array

response vector from the $\alpha_t\left(\Phi_i^t\right)$ to form the column Q_A, so that the design problem of analog precoding can be converted (see (19)).

$$T = \underset{T}{\arg\min} \left\| V_1 - A_t T \widetilde{Q}_D \right\|_F$$
$$\text{s.t.} \left\| \text{diag}\left(TT^H\right) \right\|_0 = N_t^{RF},$$
$$\text{tr}\left(A_t T \widetilde{Q}_D D_D^H T^H A_A^H\right) \le N_s \tag{19}$$

In (19), $A_t = \left[\alpha_t\left(\Phi_1^t\right), \alpha_t\left(\Phi_2^t\right), \ldots, \alpha_t\left(\Phi_L^t\right)\right]$ is a matrix of order $N_t \times L$ and sparse constrained $\left\|\text{diag}\left(TT^H\right)\right\|_0 = N_t^{RF}$ indicates that T is impossible because there are non-zero rows with more than N_t^{RF}. When T has only N_t^{RF} non-zero rows, N_t^{RF} non-zero columns in A_t can be effectively selected as the analog precoding matrix.

Eq. (19) is a sparse reconstruction problem, which can be solved by tracking the bases [6]. When the analog precoding matrix Q_A is determined, the digital precoding design problem can be converted into a minimizing problem of the F-norm (see (20)).

$$Q_D^{opt} = \underset{\widetilde{Q}_D}{\arg\min} \left\| V_1 - Q_A \widetilde{Q}_D \right\|_F$$
$$\text{s.t. tr}\left(Q_A \widetilde{Q}_D \widetilde{Q}_D^H Q_A^H\right) \le N_s \tag{20}$$

The optimal solution of Eq. (20) is presented in the form of an LS method (see (21)) [26].

$$\widetilde{Q}_D = \{Q_A\}^\dagger V_1 \tag{21}$$

Furthermore:

$$Q_D = \widetilde{Q}_D S_R = \{Q_A\}^\dagger V_1 S_R \tag{22}$$

According to the derivation of the LS matrix:

$$Q_D = \left(Q_A^H Q_A\right)^{-1} Q_A^H V_1 \tag{23}$$

According to the above analysis, the problem of selecting the optimal analog precoding matrix is a sparse reconstruction problem, which can be solved by the basic tracking principle. After obtaining the analog precoding, the LS method is used to optimize the solution method in order to obtain the optimal digital precoding matrix Q_D^{opt}.

4 Hybrid Precoding Optimization Algorithm Based on GMD

4.1 Optimization Algorithm Under Fully Connected Structure

In the fully connected structure, hybrid precoding only takes into account the base station coding, and the user receiver can perform the corresponding decoding processing based on the received signal. The optimal solution algorithm of Eq. (18) consists of two links. The first one uses the *for* loop to use the residual matrix Q_1 obtained by the GMD transformation as the optimal precoding matrix, G_1^H, substituting the OMP method as a combined matrix to obtain Q_A and Q_D. The latter performs the transformation corresponding to Lemma 1 on the Q_D and

normalizes the effective precoding matrix to meet the transmission power constraints. Algorithm 1 provides the pseudocode for the fully connected structure.

It should be pointed out that due to the calculation using the conversion relation in Lemma 1, it is not necessary to calculate S_{R} in the process, just apply the corresponding permutation and multiplication in each step of Q_D. Therefore, the computational complexity of generating Q_D is $\mathcal{O}\left(\left(N_s+N_t\right)N_s\right)$ in the reference algorithm [31], and the proposed Algorithm 1 has a complexity of $\mathcal{O}\left(\left(N_t^{\mathrm{RF}}\right)^2 N_t N_s\right)$. The Golub-Kahan double-diagonalization scheme [32] (usually the first step of calculating SVD) has a computational complexity of $\mathcal{O}\left(N_s N_t K\right)$, which shows that GMD-based hybrid precoding can optimize the algorithm complexity of spectral efficiency. Compared with the traditional SVD-based hybrid precoding, only a small additional algorithm complexity is added, because the pseudo-inverse of Q_A needs to be calculated. In terms of overall system complexity, the GMD precoding scheme using this Algorithm 1 can effectively avoid complex bit allocation problems, reduce the difficulty of encoding/decoding, and the complexity is much lower than SVD precoding schemes.

Algorithm 1: Proposed Algorithm for Fully Connected Structure

Input: The optimal precoding matrix Q_{res}, N_t^{RF}, N_t, N_r, and the array response vector-matrix A_t
Initialization: Calculate $[S_1 V_1 D_1] = \mathrm{SVD}(H)$, $[Q\,R\,P] = \mathrm{GMD}(S_1 V_1 D_1)$, $Q_{\mathrm{A}} =$ empty matrix, $Q_{\mathrm{res}} = P(:, 1:N_s)$;

1: for $i \le N_t^{\mathrm{RF}}$
2: $A_t = \frac{1}{\sqrt{N_t}} e^{j\angle S_1}$
3: $\Phi = A_t^{\mathrm{H}} Q_{\mathrm{res}}$; $k = \arg\max_{l=1,2,\ldots,L} \left(\Phi\Phi^{\mathrm{H}}\right)_{l,l}$
4: $Q_{\mathrm{A}} = [Q_{\mathrm{A}}, A_t(:,k)]$
5: $Q_D = \left(Q_A^{\mathrm{H}} Q_{\mathrm{A}}\right)^{-1} Q_A^{\mathrm{H}} A_1$
6: $Q_{\mathrm{res}} = \frac{Q_{\mathrm{res}} - Q_{\mathrm{A}} Q_D}{\left\| Q_{\mathrm{res}} - Q_{\mathrm{A}} Q_D \right\|_{\mathrm{F}}}$
7: End for
8: Generate S_{R} according to the conversion relationship of realization Lemma 1, and get $Q_D = Q_D S_{\mathrm{R}}$
9: Determine normalize $Q_D = \sqrt{N_s} \frac{Q_{\mathrm{D}}}{\left\| Q_{\mathrm{A}} Q_D \right\|_{\mathrm{F}}}$

Output: Optimized analog and digital precoding matrices Q_{A}, Q_D

4.2 Optimization Algorithm Under Partially Connected Structure

Under the partially connected structure, the previous step of the hybrid precoding optimal solution algorithm is to transform the channel H by selecting the matrix G_0 to obtain the required auxiliary matrix G [26]. In the latter step, according to the relationship between analog and digital precoding under part of the connection structure in [26], the unitary matrix obtained by the GMD transformation is used to further calculate the qualified Q_A and Q_D under the transformation, and then execute Lemma 1 corresponding transformation to normalize the effective precoding matrix to meet the constraints of transmit power. Assuming that the number of antennas connected to each chain is $M = N_t / N_t^{\mathrm{RF}}$, the base station uses K RF chains to transmit K data streams, that

is, $K = N_t^{\mathrm{RF}} = N_s$, and the base station has complete channel state information H. The specific steps are shown in Algorithm 2.

In Algorithm 2, the computational complexity of generating the auxiliary matrix G is $\mathcal{O}\left(M^2\left(N_t^{\mathrm{RF}}S + N_r\right)\right)$ [28], and the computational complexity of generating Q_D is $\mathcal{O}\left(\left(K + N_t\right)K\right)$, so the complexity of Algorithm 2 is $\mathcal{O}\left(K^2\left(N_t^{\mathrm{RF}}S + N_r\right) + K^2 + N_tK\right)$, and the algorithm complexity proposed in [6] is $\mathcal{O}\left(\left(N_t^{\mathrm{RF}}\right)^4 M + \left(N_t^{\mathrm{RF}}\right)^2 L^2 + \left(N_t^{\mathrm{RF}}\right)^2 M^2 L\right)$considering the typical millimeter-wave communication system where $N_t^{\mathrm{RF}} = 8$, $M = 8$, $N_t = 64$, $N_r = 16$, $L = 3$, $S = 5$ [26]. By analyzing the above-mentioned complexity analytical expressions, it can be seen that the complexity of the proposed algorithm is lower than that of the algorithm proposed by [21], which shows that GMD also has a better performance in the complexity of processing partial connection structure applications.

Algorithm 2: Proposed Algorithm for Partially Connected Structure

Input: Channel matrix H, number of transmitting antennas N_t, number of receiving antennas N_r
Output: Analog precoding matrix Q_{A}, a digital precoding matrix Q_D;
Initialization: Calculate $G_0 = H^{\mathrm{H}}\left(\mathrm{eye}\left(N_r\right)\right)^{-1}H$,
$G = \left[\mathrm{eye}\left(N_s\right), \mathrm{zero}\left(N_s, N_s\left(N_t^{\mathrm{RF}} - 1\right)\right)\right]G_0 \times \left[\mathrm{eye}\left(N_s\right), \mathrm{zero}\left(N_s, N_s\left(N_t^{\mathrm{RF}} - 1\right)\right)\right]^{\mathrm{H}}$

1: for $i \le N_t^{\mathrm{RF}}$
2: $[S\ V\ D] = \mathrm{SVD}\left(G\right)$
3: $[Q\ R\ P] = \mathrm{GMD}\left(SVD\right)$
4: $v_1 = P\left(:, 1\right)$
5: $\mu = R\left(1, 1\right)$
6: $a\left(:, i\right) = \dfrac{1}{\sqrt{N_t}}e^{j\angle V_1}$
7: $Q_A = a\left(:, 1\right)$
8: $d\left(i\right) = \dfrac{\mathrm{norm}\ \left(v_1, 1\right)}{\sqrt{N_t}}$
9: $p\left(:, i\right) = \frac{1}{N_s}\ \mathrm{norm}\ \left(v_1, 1\right) \times e^{j\angle v_1}$
10: $G = G - \dfrac{\left(\rho/N\sigma^2\right)\mu^2 v_1 v_1^{\mathrm{H}}}{1 + \left(\rho/N\sigma^2\right)\mu}$
11: End for
12: $Q_D = \mathrm{diag}(d)$
13: Generate S_{R} according to the conversion relationship of realization Lemma 1, and get $Q_D = Q_D S_D$
14: Normalize $Q_D = \sqrt{N_t}\dfrac{Q_D}{\left\|Q_A Q_D\right\|_{\mathrm{F}}}$

5 Simulation Results

This section analyses the performance of the GMD-based hybrid precoding scheme and spatial sparse precoding through simulation. The simulation environment is set as follows: the base station adopts ULA transmitting antenna array, the number of antennas is 64 and 256, respectively, the number of user end antennas is 16 and 64, and the antenna interval $d = \lambda/2$d. The number of RF chains at the base station and the user end are both $N_t^{\mathrm{RF}} = N_r^{\mathrm{RF}} = 8$, and the

carrier frequency is 28 GHz. Using the Saleh Valenzuela channel model, the number of effective paths is $L = 3$, the complex gain of each path obeys the distribution $CN(0, 1)$, and the azimuth angles AoA and AoD of the antennas at both ends obey $[-\pi/2, \pi/2]$. The signal to noise ratio is ρ/σ_n^2. For the optimal unconstrained precoding scheme, the water injection power allocation scheme is adopted. For all sub-channels based on SVD and GMD precoding schemes, the 16QAM modulation method is adopted.

Fig. 3 shows the spectral efficiency performance of the proposed Algorithm 1 under different iterations when the number of transmitting antennas is 256 and the number of receiving end antennas is 64. It can be seen from Fig. 3 that as the number of iterations increases, spectral efficiency gradually increases. When the number of iterations reaches 100, Algorithm 1 converges. It shows that the proposed algorithm is feasible for spectral efficiency under the GMD channel processing method.

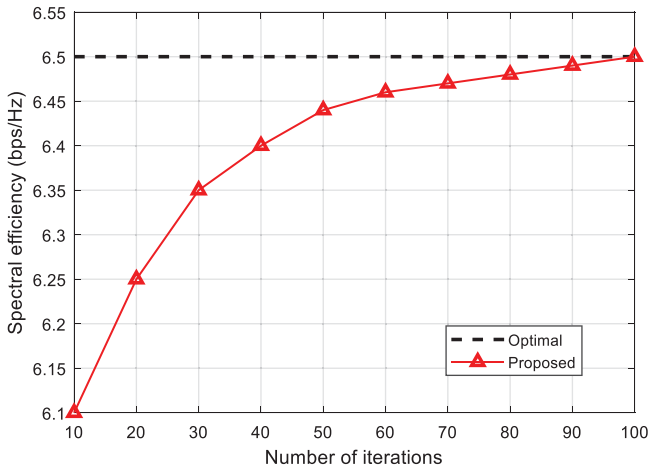

Figure 3: Comparison of spectral efficiency under different number of iterations

Fig. 4 shows the comparison of the spectral efficiency with SNR when the number of RF chains at both ends is 8 and the transmission data streams $\boldsymbol{N_s = 4}$, the number of base station antennas is different. From Fig. 4, the following conclusions are:

1) The spectral efficiency obtained by the GMD-based hybrid precoding method when the number of base station antennas is better than the reference scheme [21].
2) As the number of transmitting antennas increases, the spectral efficiency of the system gradually increases. With the increase of the SNR, the increase of the spectral efficiency becomes progressively more important, which means that the larger the scale of the antenna, the better the spectral efficiency performance, but due to the limitation of the maximum transmit power, the increase of the effect has extreme values.
3) When the number of base station antennas increases to a certain value, the proposed scheme can approach the optimal precoding performance.

Fig. 5 shows the comparison of the spectral efficiency performance with SNR in the two antenna connection modes when the number of RF chains at both ends is 8, the transmission data stream $N_s = 4$, and the number of transmitting antennas is 64. This can be seen from the results:

(1) Under the partial connection structure, the performance of the GMD-based hybrid precoding scheme is better than the traditional analog precoding;
(2) The spectral efficiency performance of the proposed precoding scheme is equivalent to the optimal precoding scheme under the partial connection structure, indicating that the proposed scheme has achieved near-optimal performance;
(3) When the SNR reaches 10 dB, the spectral efficiency of the proposed scheme under the partially connected transmission structure is approximately 80% of the scheme in [21] in the fully connected structure.

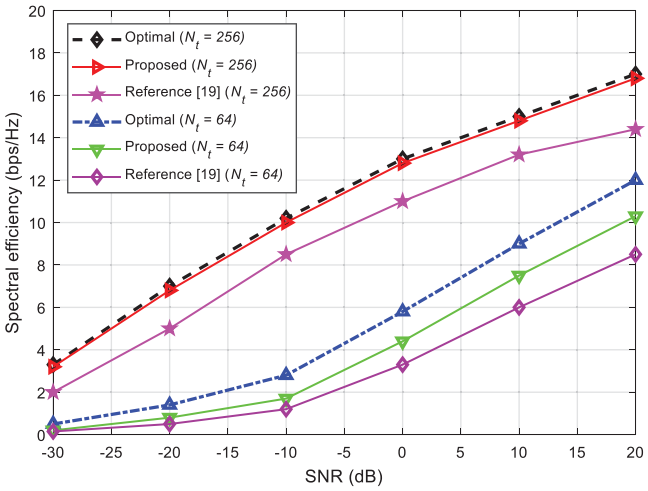

Figure 4: Spectral efficiency performance of fully connected structure system under different SNR

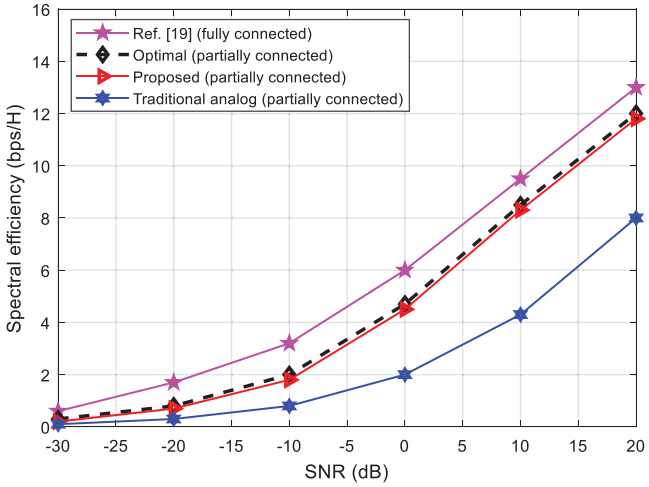

Figure 5: Spectral efficiency performance under different connection structures

Overall, the proposed system has good scalability and spectral efficiency, which guarantees the complexity of the system.

Fig. 6 compares the computational complexity of the algorithms under an increasing number of RF chains. As shown in Fig. 6, the complexity of all algorithms increases with the increasing number of RF chains. In addition, the complexity of the proposed hybrid precoding system has reduced performance compared to the optimal precoding system, which means that the proposed system is computationally efficient and requires a lower number of iterations and information signal processing time. On the other hand, the reference analog precoding scheme [21] and the traditional analog precoding scheme are very complex.

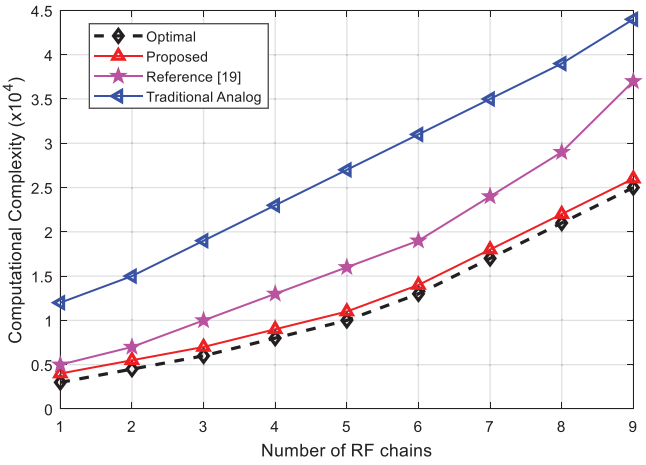

Figure 6: Complexity comparison of the algorithms vs. the number of RF chains

6 Conclusions

Millimeter wave (30 GHz–300 GHz) is used for high-speed (5G) wireless communications by allocating more bandwidth to deliver faster and higher quality video and multimedia content and services.

Due to the significant changes in the signal-to-noise ratio of the different sub-channels in the singular value decomposition, which leads to increased system complexity and encoding/decoding difficulties, a hybrid precoding scheme, which is based on geometric mean decomposition (GMD), is proposed.

Compared to the system proposed by [28], the hybrid precoding system proposed here can effectively equalize the signal-to-noise ratio of the sub-channels and reduce the overall complexity of the system. At the same time, in order to be better applied to real communication scenarios, the code has been extended to some connection transmission structures, and better frequency performance has also been obtained. The simulation results show that the frequency efficiency of the hybrid precoding scheme proposed under different base station antenna numbers is better than that of the orthogonal matching pursuit scheme [28], and that it can be applied to both existing transmission structures with a high applicability.

In perspective, the algorithms and conclusions proposed in this paper are established under ideal channel conditions. Further research is more than necessary for more complex and universal communication scenarios.

Funding Statement: The authors received no specific funding for this study.

Conflicts of Interest: The authors declare that they have no conflicts of interest to report regarding the present study.

References

[1] S. Bashir, M. H. Alsharif, I. Khan, M. A. Albreem, A. Sali *et al.,* "MIMO-Terahertz in 6G nano-communications: Channel modeling and analysis," *Computers, Materials & Continua*, vol. 66, no. 1, pp. 263–274, 2020.

[2] A. Amin, X. Liu, I. Khan, P. Uthansakul, M. Forsat *et al.,* "A robust resource allocation scheme for device-to-device communications based on Q-learning," *Computers, Materials & Continua*, vol. 65, no. 2, pp. 1487–1505, 2020.

[3] S. Alemaishat, O. A. Saraereh, I. Khan, S. H. Affes, X. Li *et al.,* "An efficient precoding scheme for millimeter-wave massive MIMO systems," *Electronics*, vol. 8, no. 9, pp. 1–15, 2019.

[4] A. Silva, S. Teodoro, R. Dinis and A. Gamero, "Iterative frequency-domain detection for IA-precoded MC-CDMA systems," *IEEE Transactions on Communications*, vol. 62, no. 4, pp. 1240–1248, 2014.

[5] A. Al-Nimrat, M. Smadi, O. A. Saraereh and I. Khan, "An efficient channel estimation scheme for mmwave massive MIMO systems," in *Proc. IEEE Int. Conf. on Communication, Networks and Satellite (ComNetSat)*, Makassar, Indonesia, pp. 1–8, 2019.

[6] A. Silva, J. Assuncau, R. Dinis and A. Gameiro, "Performance evaluation of IB-DFE based strategies for SC-FDMA systems," *EURASIP Journal on Wireless Communications and Networking*, vol. 13, pp. 1–10, 2013.

[7] I. Khan and D. Singh, "Efficient compressive sensing based sparse channel estimation for 5G massive MIMO systems," *AEU-International Journal of Electronics and Communications*, vol. 89, no. 2, pp. 181–190, 2018.

[8] D. Casthanheira, A. Silva, R. Dinis and A. Gameiro, "Efficient transmitter and receiver design for SC-FDMA based heterogeneous networks," *IEEE Transactions on Communications*, vol. 63, no. 7, pp. 2500–2510, 2015.

[9] M. H. Zafar, I. Khan and M. Basheri, "Matrix inversion-less direct decoding for efficient channel estimation fifth-generation massive MIMO systems," *IET Communications*, vol. 14, no. 5, pp. 865–871, 2020.

[10] D. Castanheira, A. Silva and A. Gameiro, "Set optimization for efficient interference alignment in heterogeneous networks," *IEEE Transactions on Wireless Communications*, vol. 13, no. 10, pp. 5648–5660, 2014.

[11] I. Khan, J. Rodrigues, J. Al-Muhtadi, M. I. Ktk, Y. Jan *et al.,* "A robust channel estimation scheme for 5G massive MIMO systems," *Wireless Communications and Mobile Computing*, vol. 3469413, pp. 1–9, 2019.

[12] S. Teodoro, A. Silva, R. Dinis, F. Barradas, P. M. Cabral *et al.,* "Theoretical analysis on nonlinear amplification effects in massive MIMO systems," *IEEE Access*, vol. 7, pp. 172277–172289, 2019.

[13] A. Amin, X. H. Liu, M. A. Saleem, S. Henna, T. Islam *et al.,* "Collaborative wireless power transfer in wireless rechargeable sensor networks," *Wireless Communications and Mobile Computing*, vol. 9701531, no. 9, pp. 1–13, 2020.

[14] T. S. Rappaport, S. Sun, R. Mayzus, H. Zhao, Y. Azar *et al.,* "Millimeter wave mobile communications for 5G cellular: It will work!," *IEEE Access*, vol. 1, pp. 335–349, 2013.

[15] J. Zhang, L. Dai, X. Li, Y. Liu and L. Hanzo, "On low-resolution ADCs in practical 5G millimeter-wave massive MIMO systems," *IEEE Communications Magazine*, vol. 56, no. 7, pp. 205–211, 2018.

[16] B. Wang, F. Gao, S. Jin, H. Lin and G. Y. Li, "Spatial- and frequency-wideband effects in millimeter-wave massive MIMO systems," *IEEE Transactions on Signal Processing*, vol. 66, no. 13, pp. 3393–3406, 2018.

[17] Z. Gao, L. Dai, D. Mi, Z. Wang, A. M. Imran *et al.,* "Mmwave massive-MIMO-based wireless backhaul for the 5G ultra-dense network," *IEEE Wireless Communications*, vol. 22, no. 5, pp. 13–21, 2015.

[18] H. Haneche, B. Boudraa and A. Ouahabi, "A new way to enhance speech signal based on compressed sensing," *Measurement*, vol. 151, no. 1, pp. 107–117, 2020.

[19] Y. Jiang, W. W. Hager and J. Li, "The geometric mean decomposition," *Linear Algebra and Its Applications*, vol. 396, pp. 373–384, 2005.

[20] H. Haneche, A. Ouahabi and B. Boudraa, "New mobile communication system design for Rayleigh environments based on compressed sensing-source coding," *IET Communications*, vol. 13, no. 15, pp. 2375–2385, 2019.

[21] O. E. Ayach, S. Rajagopal, S. A. Surra, Z. Pi and R. W. Heath, "Spatially sparse precoding in millimeter wave MIM systems," *IEEE Transactions on Wireless Communications*, vol. 13, no. 3, pp. 1499–1513, 2014.

[22] J. A. Tropp and A. C. Gilbert, "Signal recovery from random measurements via orthogonal matching pursuit," *IEEE Transactions on Information Theory*, vol. 53, no. 12, pp. 4655–4666, 2007.

[23] A. Kaushik, J. Thompson and M. Yaghoobi, "Sparse hybrid precoding and combining in millimeter wave MIMO systems," in *Proc. Radio Propagation and Technologies for 5G*, Durham, UK, pp. 1–7, 2016.

[24] A. Ahrens, C. B. Peces and F. C. Broncano, "Power allocation in SVD-and GMD-assisted MIMO systems," *Optimization and Engineering*, vol. 17, no. 4, pp. 919–940, 2016.

[25] H. C. Chen and Y. P. Lin, "Differential feedback of geometrical mean decomposition precoder for time-correlated MIMO systems," *IEEE Transactions on Signal Processing*, vol. 65, no. 14, pp. 3833–3845, 2017.

[26] X. Gao, L. Dai, S. Han, I. C. Lin and R. W. Heath, "Energy-efficient hybrid analog and digital precoding for mmwave MIMO systems with large antenna arrays," *IEEE Journal on Selected Areas in Communications*, vol. 34, no. 4, pp. 998–1009, 2016.

[27] P. V. Amadori and C. Masouros, "Low RF-complexity millimeter-wave beamspace-MIMO systems by beam selection," *IEEE Transactions on Communications*, vol. 63, no. 6, pp. 2212–2223, 2015.

[28] E. Bjornson, E. G. Larsson and M. Debbah, "Massive MIMO for maximal spectral efficiency: How many users and pilots should be allocated," *IEEE Transactions on Wireless Communications*, vol. 15, no. 2, pp. 1293–1308, 2016.

[29] C. L. Chao, S. H. Tsai and T. Y. Hsu, "Bit allocation schemes for MIMO equal gain precoding," *IEEE Transactions on Wireless Communications*, vol. 10, no. 5, pp. 1345–1350, 2011.

[30] Z. Xiong and Z. Liu, "The forward order law for least square-inverse of multiple matrix products," *Mathematics*, vol. 7, no. 3, pp. 1–10, 2019.

[31] Y. Jiang, J. Li and W. W. Harger, "Joint transceiver design for MIMO communications using geometric mean decomposition," *IEEE Transactions on Signal Processing*, vol. 53, no. 10, pp. 3791–3803, 2005.

[32] A. Goldsmith, S. A. Jafar, N. Jindal and S. Vishwanth, "Capacity limits of MIMO channels," *IEEE Journal on Selected Areas in Communications*, vol. 21, no. 5, pp. 684–702, 2003.